Rossby waves impact on persistent oxic and suboxic chlorophyll maxima in the Eastern Tropical North Pacific

Amaru Márquez-Artavia,[1-5,] Xiomara M. Márquez-Artavia,[2] Juan P. Salazar-Ceciliano,[2] Laura Sánchez-Velasco,[3] Emilio Beier,[1] Aurélien Paulmier[4]

[1]Laboratory of Marine Macroecology CONACyT, Ensenada Center for Scientific Research and Higher Education, Ensenada, Mexico; [2]Department of Physics, National University of Costa Rica, Heredia, Costa Rica; [3]Department of Plankton and Marine Ecology, National Polytechnic Institute - Interdisciplinary Center in Marine Sciences, La Paz, México; [4]Laboratory of Space Geophysical and Oceanographic Studies, CNRS/IRD/UPS/CNES, Toulouse, France; [5]School of Biology, National University of Costa Rica. Heredia, Costa Rica

Corresponding author: Xiomara M. Márquez-Artavia, Department of Physics, National University of Costa Rica, Heredia, Costa Rica.
E-mail: xiomara.marquez.artavia@una.ac.cr

Key words: chlorophyll-a maxima, Oxygen Minimum Zones, isopycnal movement, BGC-Argo float, Rossby waves.

Authors' contributions: all the authors made a substantive intellectual contribution. All the authors have read and approved the final version of the manuscript and agreed to be held accountable for all aspects of the work.

Conflict of interest: the authors declare no potential conflict of interest.

Funding: AM acknowledges the financial support received from CONACyT as research assistant no. 19337 to conduct this work. EB was supported by the project Dinámica y Termodinámica de la Corriente Occidental Mexicana (CICESE 612-691) while LSV acknowledges support from the Instituto Politécnico Nacional (SIP-IPN 20200669), and CONACyT during the sabbatical.

Availability of data and materials: all data generated or analyzed during this study are included in this published article.

Acknowledgments: the data from the floats were collected and made freely available by the international Argo project and the national programs contributing to it (http://doi.org/10.17882/42182). We extended our gratitude to the Principal Investigators of the Argo program and acknowledged the availability of SLA, wind data, as well as the EN4.2.1 datasets from Copernicus Marine Service (http://marine.copernicus.eu), Remote Sensing Systems (www.remss.com) and Met Office-UK (https://www.metoffice.gov.uk/hadobs/en4/). The authors express their gratitude to Dr. William Kessler for suggesting to the representation of chlorophyll in density space. Additionally, we are extremely thankful for the insightful comments provided by Professor Paulo Polito and the anonymous reviewers, which substantially improved this work.

Received: 9 March 2024.
Accepted: 3 June 2024.

Publisher's note: all claims expressed in this article are solely those of the authors and do not necessarily represent those of their affiliated organizations, or those of the publisher, the editors and the reviewers. Any product that may be evaluated in this article or claim that may be made by its manufacturer is not guaranteed or endorsed by the publisher.

Licensee PAGEPress, Italy
Advances in Oceanography and Limnology, 2024; 15:11301
DOI: 10.4081/aiol.2024.11301

ABSTRACT

This study aims to describe the response of two persistent chlorophyll-*a* maxima to physical processes that affect the position of the thermocline/nitracline in the Eastern Tropical North Pacific (ETNP). We focused on Long Rossby Waves (LRWs) due to their relevance to the ETNP circulation and their potential role in introducing nutrients into the euphotic zone. We found that the shallower chlorophyll-*a* maximum in oxygenated waters became more intense when denser waters (containing more nutrients) moved toward the surface. This suggests that changes in isopycnals and nitracline displacements modify nutrient supply in the euphotic zone, leading to changes in phytoplankton growth. The suboxic and deeper chlorophyll-*a* maximum showed a strong association with the 26 kg m^{-3} isopycnal, which was only mechanically displaced, and its chlorophyll-*a* content did not seem to covary with irradiance or nutrients. The decorrelated responses of the chlorophyll-*a* maxima could be explained if different phytoplankton groups are associated with them. LRWs can affect the position of the thermocline/nitracline and isopycnals in an annual cycle, but it seems to be a "background" signal modulated by higher frequency processes such as mesoscale eddies and other Rossby waves. The co-occurrence of processes can control the nitracline depth, and thus the input of nutrients into the euphotic zone, leading to sporadic enhancements in chlorophyll-*a* concentration in one maximum.

Introduction

Photosynthesis is a key process for life on the planet, it provides food with the primary producers, and oxygen for the majority of the heterotrophs, it is controlled by both catabolic (light) and anabolic (nutrients) requirements (Rabinovich, 1969).

The process of photosynthesis produces biomass, typically rich in carbon or nitrogen. This biomass can be found in pigments like chlorophyll-*a*. Phytoplankton, which are photosynthetic organisms, contain chlorophyll. The highest Chlorophyll concentration is found in parts of the water where there is plenty of sunlight, allowing photosynthesis to happen more effectively. However, the amount of chlorophyll in the ocean can change due

to factors like the availability of nutrients, water temperature, and ocean movements (Lalli *et al*., 2006)

Chlorophyll-*a* maxima are significant aspects of the pelagic ecosystem, originating from several processes. For instance, they may develop near the nitracline due to an increase in the phytoplankton growth: coinciding with biomass peaks typically occurring in stratified waters with mesotrophic or eutrophic conditions (Cullen, 2015). Chlorophyll-*a* maxima can also arise through photoacclimation: wherein phytoplankton increase their intracellular pigment concentration in response to the low-light availability (Mignot *et al*., 2014; Cullen, 2015). This case is commonly found in oligotrophic regions, and the chlorophyll-*a* maximum only represents changes in the pigment concentration, not in biomass.

The Eastern Tropical North Pacific (ETNP) region strongly influenced by wind jets, ocean currents, and the ENSO phenomenon. One of the characteristics of the ETNP is its prominent thermocline and nutricline, which directly affect marine life. In Oxygen Minimum Zones (OMZs), such as the Eastern Tropical North Pacific (ETNP) and the Arabian Sea, multiple chlorophyll-*a* maxima can develop in the water column (Goericke *et al*., 2000; Lavin *et al*., 2010; Garcia-Robledo *et al*., 2017; Márquez-Artavia *et al*., 2019). One chlorophyll-*a* maximum forms near the nutricline in well-oxygenated waters, while another develops below the nutricline, in the lower part of the euphotic zone, and within suboxic waters (<20 $\mu molO_2\ kg^{-1}$). This suboxic maximum is caused by an increase in the cell number of *Prochlorococcus* ecotypes specific to the OMZs (Goericke *et al*., 2000; Lavin *et al*., 2010). This chlorophyll-*a* maximum is significant biogeochemically because it serves as a source of locally consumed organic matter and oxygen (Garcia-Robledo *et al*., 2017). However, little is known about the physical mechanisms influencing and sustaining phytoplankton populations.

Various physical processes affecting phytoplankton populations have been discussed in the literature, including the impacts of mesoscale eddies and the Long Rossby Waves (LRWs) (Siegel *et al*., 1999; Uz *et al*., 2001; Killworth *et al*., 2004; McGillicuddy, 2016). Both processes alter the vertical distribution of properties such as nutrients, oxygen, and chlorophyll-*a* (Sakamoto et al., 2004; McGillicuddy et al., 2007; McGillicuddy, 2016), albeit on different spatial (~900 km) and temporal scales (~1 year). The effects of LRWs on chlorophyll-*a* distribution can be either physical or biological (Killworth *et al*., 2004). Physical effects encompass mechanical displacements through horizontal or vertical advection (Killworth et al., 2004; Belonenko *et al*., 2018), while biological processes relate to phytoplankton responses to the nutrient availability and light., Uz *et al*. (2001) suggested that LRWs may transport nutrients into the euphotic zone, thereby promoting an increase in chlorophyll-*a* concentration.

In the Arabian Sea OMZ, LRWs have been observed to alter the depth and intensity of the two chlorophyll-*a* maxima, one of which sporadically occurs within the suboxic waters (Ravichandran *et al*., 2012). In the ETNP, LRWs are recognized as a significant factor in regional circulation, controlling the thermocline position on seasonal scales (Kessler, 1990, 2006). Despite extensive reviews of chlorophyll-*a* and primary productivity in the ETPN (Pennington *et al*., 2006), the effects of LWRs on chlorophyll-a maxima have not yet been evaluated. Furthermore, Pennington *et al*. (2006) did not consider the formation and variability of the chlorophyll-*a* maximum found in suboxic waters, a persistent feature in some regions of the ETNP (Márquez-Artavia *et al*., 2019).

This study aims to describe the temporal evolution of phytoplankton communities indicated by the chlorophyll-*a* concentration in the ETNP OMZ, utilizing high-resolution data from a Biogeochemical Argo float (BGC-Argo float) with a relatively long record. This data set allows for a more detailed resolution of processes than the monthly climatology of the ship and satellite-based on observations used previously by Pennington *et al*. (2006). We particularly focus on LRWs due to their significance at 13ºN and their potential as a mechanism for introducing nutrients into the euphotic zone. Considering this, we test the following hypothesis: when LRWs displace isopycnals towards the surface (cyclonic phase) they will increase the nutrient supply into the euphotic zone, thereby stimulating phytoplankton growth. Conversely, the opposite scenario is anticipated when LRWs deepen the isopycnals around 60 m (anti-cyclonic phase).

Materials and methods

Data sources

We used vertical profiles collected by a BGC Argo Float (WMO3901531) from November 30th, 2016 to March 10th, 2019. The float was deployed at 110°W and 13°N, programmed to surface at local noon after drifting for five days at a depth of 1000 meters. Although the BGC-Argo float trajectory exhibited several loops, most stations concentrated along the east-west axis with a mean position at 112.16°W and 13.19°N (Figure 1). This predominantly zonal trajectory enabled us to compare it with latitudinal-dependent phenomena such as Rossby waves.

The float was sampling in oceanic waters where the mean surface chlorophyll-a concentration was slightly above 0.1 mg m-3 (Figure 1), which corresponds to mesotrophic conditions according to the classification of Antoine *et al.* (1996). Notably, the float´s trajectory lay between the western flank of an anticyclonic circulation known as the Tehuantepec Bowl (centered at 13ºN and 105ºW), and the onset of the North Equatorial Current, which manifests as a zonal flow west of 125ºW (Figure 1). The mean speed of the float, estimated from station locations and time was 3.6±2.3 cm s^{-1}, akin to the speed at 1000 m depth (2.88±1.70 cm s^{-1}) in the ANDRO dataset (Ollitrault and Rannou, 2013). Consequently, the float sampled along the boundaries of the ETNP, with its trajectory predominantly influenced by intermediate-depth currents, typical of an instrument drifting for five days at 1000 m.

The WMO3901531 BGC-Argo float is equipped with sensors to measure temperature, salinity, oxygen, chlorophyll-*a* fluorescence, light backscattering at an angle of 124º at two wavelengths (532 and 700 nm.), and irradiance in several channels (380, 412, 490 nm and integrated into the Photosynthetically Active Radiation spectral band, PAR). Given the diverse sampling schemes and resolutions of each sensor, we employed synthetic profiles where all variables are reported on the same pressure axis. The detailed procedure for constructing these synthetic profiles can be found in Bittig *et al*. (2018), and the data are accessible from the Coriolis Global Data Assembly Center (ftp://ftp.ifremer.fr/ifremer/argo/etc/argo-synthetic-profile).

Sea Surface Level Anomalies

Sea Surface Level Anomalies (SLA) from the delayed mode multi-mission altimeter gridded fields Level-4, with a resolution of 0.25ºx0.25º from January 1st, 2014 to May 13th, 2019, were obtained from the Copernicus Marine Environment Monitoring Service (http://marine.copernicus.eu). We utilized SLA data to investigate whether the observed variability in the float time series could be linked to oceanographic phenomena at meso and large scales, such as eddies and Rossby waves. The phase speed of LRWs was calculated from a longitude-time diagram, whereby lines following slanted features were visually defined and their slopes estimated (Barron *et al*., 2009, Glatt *et al*., 2011).

Mesoscale eddies

To identify mesoscale eddies, we employed the py-eddy-tracker software, which detects eddies based on closed contours of SLA (Mason *et al*., 2014). Closed contours were computed at 1 cm intervals within the range of -100 to 100 cm. Each closed contour was compared with a fitted circle with the same area, and the shape error, defined as the sum of the areas deviating from the fitted circle, was expressed as a percentage of the total area (Kurian *et al*., 2011). Criteria for identifying eddies included ensuring the shape error did not exceed 55%, the number of pixels within the closed contour should be between 8 and 100, all SLA values were either above or below those defined by the closed contour, there was only a local maximum or minimum within the closed contour and, the amplitudes ranged from 1 to 150 cm. Eddies defined by the closed contours tended to be irregular rather than perfect circles, delineating an effective contour, used to determine whether the BGC-Argo float was within or outside a given structure. Additionally, eddy identification was conducted on raw SLA, without screening based on any eddy characteristics such as lifespan or size.

BGC-ARGO float data handling

We used temperature and salinity records from the synthetic profiles to compute absolute salinity, conservative temperature, and the potential density anomaly relative to the surface, employing the thermodynamic equation of seawater, TEOS-10 (Mcdougall and Barker, 2017). The depth of the 20 °C isotherm (Z20) was selected as a proxy of the thermocline depth for comparison with model predictions, following the precedent set by Kessler (1990, 2006). Additionally, we calculated the pycnocline depth to demonstrate how Z20 reflects the dynamics of the pycnocline in ETNP near 13°N, determined as the maximum gradient of density relative to depth.

We derived the vertical distribution of nitrate using temperature, salinity, oxygen, geographical position, and profile dates obtained by the BGC-ARGO float, employing the CANYON algorithm developed by Sauzède *et al*. (2017). While CANYON provides a convenient method of estimating nitrate concentration when direct measurements are unavailable, it tends to produce biased estimations in the OMZ, likely due to its inability to accurately represent denitrification processes in oxygen-deficient waters. Consequently, we only used the CANYON nitrate profiles to determine the nitracline depth, calculated as the maximum vertical gradient. The depths of Z20, pycnocline, and nitracline were then correlated using Pearson's coefficient.

Calculations of the annual cycles

The annual cycles Z20, pycnocline, nitracline, and the chloro-

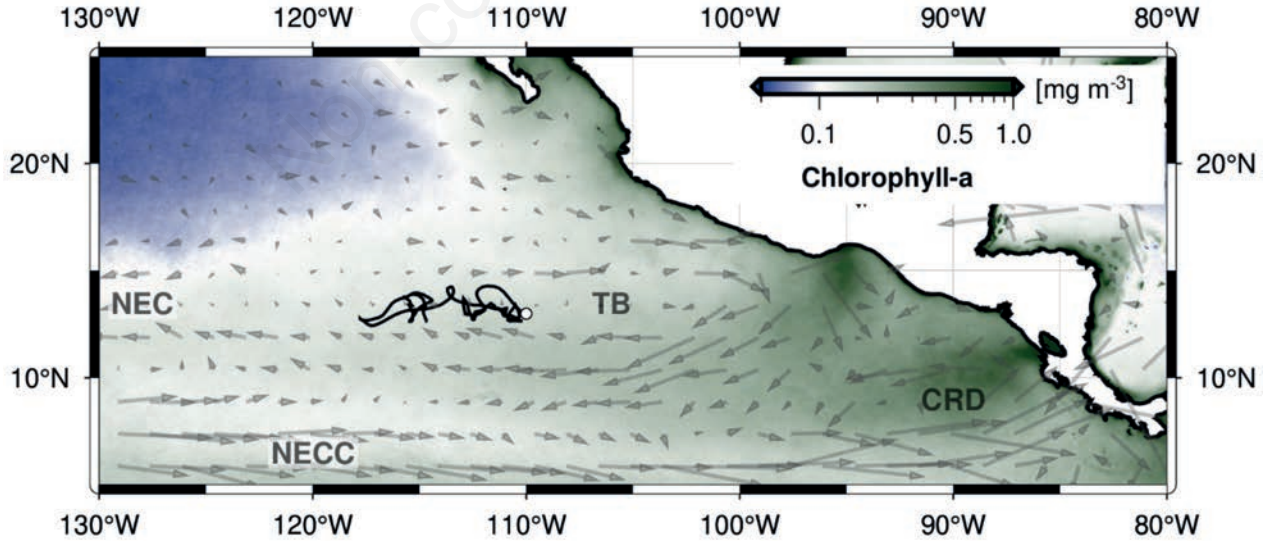

Figure 1. Representation of main oceanographic features of the Eastern Tropical North Pacific (ETNP) and the trajectory of the BGC-Argo float. Surface chlorophyll-a measured by satellite radiometers and geostrophic currents from altimetry were averaged using the 2014-2018 period. The white point represents the deployment location of the float and the black line its trajectory. The position of the North Equatorial Counter Current (NECC), Costa Rica Dome (CRD), Tehuantepec Bowl (TB) and the North Equatorial Current are also indicated. Chlorophylll-*a* data correspond to the version 5 of the ESA-CCI ocean color product (Sathyendranath *et al.* 2019).

phyll-*a* concentration were obtained by least squares fitting of a sinusoidal function such as:

$$y(t) = \underline{y} + A\cos(\omega t - \phi)$$

where $\underline{y}$ is the mean of the record estimated from the fitting, A and ϕ denote coefficients indicating the amplitude and phase of the cosine function, respectively, while ω represents the angular frequency ($2\pi/365.25$ days) and *t* signifies time. The least-square fitting was conducted according to Ripa (2002) to obtain uncertainties of the coefficients.

Chlorophyll-*a* data

Chlorophyll-*a* derived from fluorescence and light backscattering was processed and quality controlled by the Argo Data Management Team (Schmechtig *et al*., 2018; Schmechtig *et al*., 2019; Schmechtig *et al*., 2023). For chlorophyll-*a* fluorescence, this process involved negative spike removal, non-photochemical quenching correction, and the application of a global correction factor to obtain the least biased estimation of chlorophyll-*a,* as described by Roesler *et al*. (2017). Regarding light backscattering, the Argo program estimates the particle backscattering coefficient (b_{bp}) at single angles following the methodology of Boss & Pegau (2001), with quality control also incorporating negative spike removal. Although the BGC-float measures b_{bp} at 532 and 700 nm, only the latter was used as a proxy of particulate organic carbon or phytoplankton biomass due to its lesser sensitivity to pigment and dissolved material absorption in seawater (Boss & Häentjens, 2016). We smoothed the chlorophyll-*a* and bbp700 data by using two consecutive running median filters of five and seven points (Briggs *et al*., 2011; Rembauville et al., 2017). Given the mean vertical resolution of the synthetic profiles (0.8 m), this process is equivalent to averaging in layers of approximately four and six meters.

The quality control of irradiance in the Argo program involves a global test to identify values outside the expected range (Poteau *et al*., 2019). Additionally, we implemented the protocol described by Organelli *et al*. (2016). Following this quality control, only 32% of the profiles measured at PAR were deemed acceptable quality (good or probably good). We considered this a percentage too low. Consequently, we derived profiles of PAR irradiance based on the Lambert-Beer law, estimating the attenuation coefficient (KDPAR) and the irradiance just below the surface (EPAR0-) from the measurement at 490 nm, in which 64% of the profiles were deemed of acceptable quality.

EPAR0- represents an instantaneous value. To ascertain the daily light regime of phytoplankton, we integrated over the length of a day at the float´s location, following the procedure described by Mignot *et al*. (2018). At the conclusion of this procedure, we obtained profiles of daily integrated irradiance, which served two purposes: i) to compute the euphotic zone depth based on the depth of an isolume, ii) to get the daily integrated irradiance received at the depth of the chlorophyll-*a* maxima alongside the BGC-Argo float time series.

The euphotic zone was defined by the depth of the 0.04 molQ m^{-2} day^{-1} isolume corresponding to an instantaneous PAR irradiance of 1 µmolQ m^{-2} s^{-1}, assumed constant for 12 hours. The light level was chosen as the mean compensation irradiance estimated for low-light adapted ecotypes of *Prochlorococcus* (Moore *et al*., 1995). that the 12-hour assumption aligns with the daytime duration at the mean float position, and is consistent with the conditions used in laboratory experiments to assess *Prochlorococcus* photo-physiology.

The vertical distribution of chlorophyll-*a* in the OMZ of the ETNP frequently exhibits two maxima, although profiles with a single maximum or with a more complex distribution are also observed (Márquez-Artavia *et al*., 2019). All these cases were observed in the analyzed dataset used in this work, some representative profiles are shown in Figure 2. Nonetheless, we focused on profiles with single or double maxima to analyze the evolution of the physical and biogeochemical conditions related to them.

We obtained the oceanographic conditions associated with the chlorophyll-*a* maxima by considering the shape of the chlorophyll-*a* profile, defined by a fitting function with one or two Gaussian curves (one for each maximum) plus an exponential decay. Similar approaches have been used elsewhere in the literature (Mignot *et al*., 2011; Muñoz-Anderson *et al*., 2015; Barbieux *et al*., 2018). We fitted the functions with the Levenberg-Marquardt algorithm to determine the parameters defining the depth and width of the chlorophyll-*a* maxima. The depth of each maximum corresponds to the center of the Gaussian curve, while the width covers the region between the center ±1 standard deviation. Properties such as chlorophyll-*a*, and PAR, were represented by averaging the values within the width of each maximum. Linear correlations between variables were calculated using Pearson's coefficient.

At each time step, the conditions related to each maximum are defined by the values of chlorophyll-*a* (chla), $b_{bp}700$ (as a proxy of carbon or phytoplankton biomass: b_{bp}), the depth of the nitracline (Z_nitracline), Dissolved Oxygen (DO), downwelling irradiance at PAR (PAR) and the ratio between $b_{bp}700$ and chlorophyll-*a,* which serves as a proxy for the carbon to chlorophyll-*a* ratio (b_{bp}:chla). We used Z20 to identify how the conditions of the chlorophyll-*a* maxima were related to the thermocline/nitracline movements.

Principal Component Analysis

To identify patterns of co-variability, and decompose the temporal evolution of the chlorophyll-*a* maxima conditions into a set of uncorrelated modes, we performed a Principal Component Analysis (PCA). The eigenvalues and eigenvectors were obtained by singular value decomposition of the standardized data. Individual observations were discarded if at least one of the variables did not have valid data. PCA was conducted using the FactoMine package version 1.42 in R 3.5.3 (Sébastien *et al*., 2008; R Core Team, 2019).

Long Rossby Wave model

We used a simple analytical linear model to simulate the thermocline depth influenced by LRWs, which accounts for both the local effects of wind stress on the thermocline depth and the remote effects caused by the propagation of perturbations (Kessler, 2006). This simplified linear model has been employed in several previous studies and successfully replicates the propagation of Long baroclinic Rossby waves in tropical regions. It explains the observed annual cycle of Z20 in the entire ETNP, and it has toadied in understanding the local circulation of the Pacific off Mexico (Kessler, 2006; Godínez *et al*., 2010; Watanabe *et al*., 2016). Most

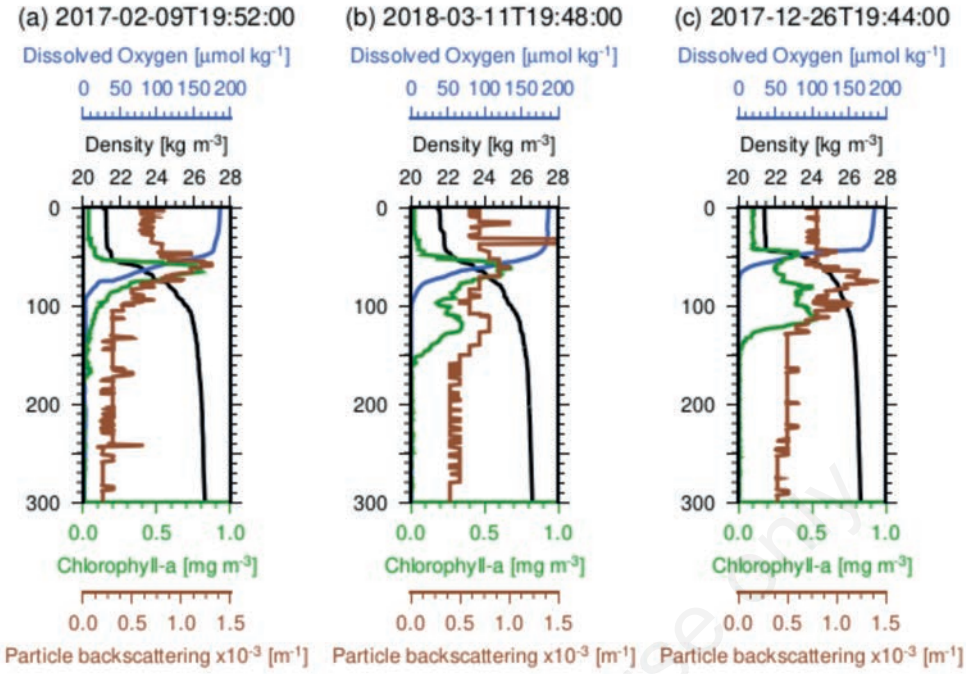

Figure 2. Representative vertical profiles gathered by the BGC-Argo float. It is shown examples where the chlorophyll-*a* presented one (a), two (b) and three maxima (c). It is also shown the vertical distribution of density, dissolved oxygen and particle backscattering (proxy of phytoplankton biomass). Note that chlorophyll-a and particle backscattering maxima coincided in depth.

of these prior studies involved comparing the model with observations. Given the correspondence between the model and observations, they concur that LRWs are a significant physical process in explaining the dynamic of the ETNP, and particularly the low-frequency variability of the thermocline.

In line with the methodology of the studies, as mention before, we employed the model to compare the simulated thermocline depth (Z20) with the observations from BGC-Argo float in the ocean interior and with satellite altimeter measurements of SLA at the surface. These comparisons were conducted considering the baroclinic nature of LRWs implying that the surface expression as SLA is also observed as thermocline movements. Additionally, we computed the Ekman pumping velocity to compare and cross-correlate it with Z20. This enables us to assess whether thermocline movements can be solely explained by local wind forcing. Ekman pumping velocity was computed daily for the dates sampled by the BGC-Argo float (Bernades *et al*., 2021) using the CCMP version 2 data product (Li *et al*., 2021) with a spatial resolution of 0.25°x0.25°. It was linearly interpolated to the BGC-Argo float positions and the highest correlation and lag were reported.

Results

Sea Level Anomalies and the westward propagation of signals

The spatial and temporal variability of SLA exhibited three prominent features around the BGC-Argo float locations. Firstly, there was a large-scale process annual period: In May 2017, the BGC-ARGO floats sampled within a region of positive SLA values spanning more than 8000 km in longitude (8-15ºN and 80-130ºW; Figure 3a), transitioning to negative SLA after six months and with a similar spatial pattern (Figure 3b). Secondly, this signal seemed to originate in the east and propagate westward, manifesting as slanted features in the longitude-time diagrams of the SLA (Figure 3c). Thirdly, the westward propagating signals showed an estimated phase speed of 13.1±1.6 km day^{-1} (Figure 3c), akin to values reported near 13ºN by Chelton and Schlax (1996). In summary, SLA displayed an annual signal with westward propagation and a phase speed characteristic of LRWs.

Interestingly, the evolution of SLA and its LRW-like characteristics coincided with the temporal variability of chlorophyll-*a* depicted in Figure 4. The time series revealed two persistent chlorophyll-*a* maxima changes in depth over time. During the period of positive SLA (*e.g.* May 2017), the chlorophyll-a maxima were deeper, while in the negative period (*e.g.* November 2017) they were shallower (Figures 4a and 4b). Both chlorophyll-*a* maxima exhibited depth changes of approximately 40 m with a nearly annual signal, tracking the movements of Z20, the pycnocline, and nitracline (Figure 4b). Notably, the shallower maximum showed an increase in chlorophyll-*a* content when the pycnocline, Z20, and nitracline moved towards the surface, while the deeper maximum showed minimal changes in pigment concentration over the record but generally remained within the euphotic zone (Figure 4b).

Given the differing positions of the chlorophyll-*a* maxima in the water column, variations in other properties were expected. For instance, we observed that the shallower maximum occurred in more oxygenated waters (112.4±31 µmolO_2 kg^{-1}) compared to the deeper chlorophyll-*a* maximum (0.8±0.8 µmolO_2 kg^{-1}). Based

on this difference in the dissolved oxygen concentration, we termed each Chlorophyll-*a* Maximum (CM) as the oxic-CM and the suboxic-CM respectively. It is worth noting that while profiles with one or several maxima were observed (Figure 2), they accounted for only 3.1% of the good quality profiles analyzed in this study, with the case of two maxima dominating, and found in 96.9% of cases.

To discern whether the chlorophyll-*a* maxima resulted from phytoplankton growth enhancements or photoacclimation, we also examined the temporal evolution of $b_{bp}700$ a proxy for organic carbon or phytoplankton biomass (Stramski *et al*., 2004; Martinez-Vicente *et al*., 2013; Boss *et al*., 2015; Rasse *et al.*, 2017). Both the oxic and suboxic-CM coincided with peaks in the $b_{bp}700$ or biomass (Figure 2 and 4c). Chlorophyll-*a*, $b_{bp}700$ and dissolved oxygen at each maximum exhibited a nearly annual signal in their depth displacements (Figure 4). Person's correlation coefficients between the time series of chlorophyll-*a* and bbp700 were 0.76 (n=153, df=151, p-value <0.05) for the oxic-CM, and 0.89 (n=149, df=147, p-value <0.05) for the suboxic-CM. The nearly annual oscillation was observed in other properties such as density and oxygen (Figure 5).

Chlorophyll-*a* on density coordinates and effects of Long Rossby Waves

As illustrated above, the two persistent chlorophyll-*a* and $b_{bp}700$ maxima (oxic-CM and suboxic-CM) exhibited depth variations simultaneously (Figure 4). However, in the density space, both maxima responded differently (Figure 5a). The oxic-CM (shallower and in less dense water) showed sparse distribution in the density space, moving between isopycnal surfaces throughout the year (Figure 5a). In May 2017, the oxic-CM resided in water with a density lower than 23 kg m^{-3} at approximately 70 m depth, with a thickness of approximately 20 m. Subsequently, it moved to denser waters, reaching the 25 kg m^{-3} isopycnal in November 2017, where it became wider and shallower (Figures 4 and 5a). By contrast, the suboxic-CM displayed low variability in density, remaining near the 26 kg m^{-3} isopycnal throughout the record (Figure 5a).

Based on the results, the response of each maximum to the pycnocline displacements differ, though they could be associated with isopycnal movements caused by the propagation of LRWs. Considering the large-scale spatial pattern of SLA (Figure 3a and b), and the nearly annual oscillation observed in the pycnocline depth (Figure 4), LRWs as regarded as a potential mechanism, as discussed in previous works (Kessler, 1990, 2006).

The analytical model presented in section 2 was then employed to assess if the observed Z20 followed the theoretical prediction caused by the propagation of LRWs. Notably, the mean position of Z20 from the fitting procedure was 78.67±0.72 m. with an annual harmonic amplitude and phase of 19.25±1.01 m and 2.32±0.05 radians, respectively. This annual signal of Z20 closely matches the model results. accounting for 61.5 % of the total variance observed of Z20. Although the direct effect of the wind-induced Ekman pumping could serve as an alternative explanation

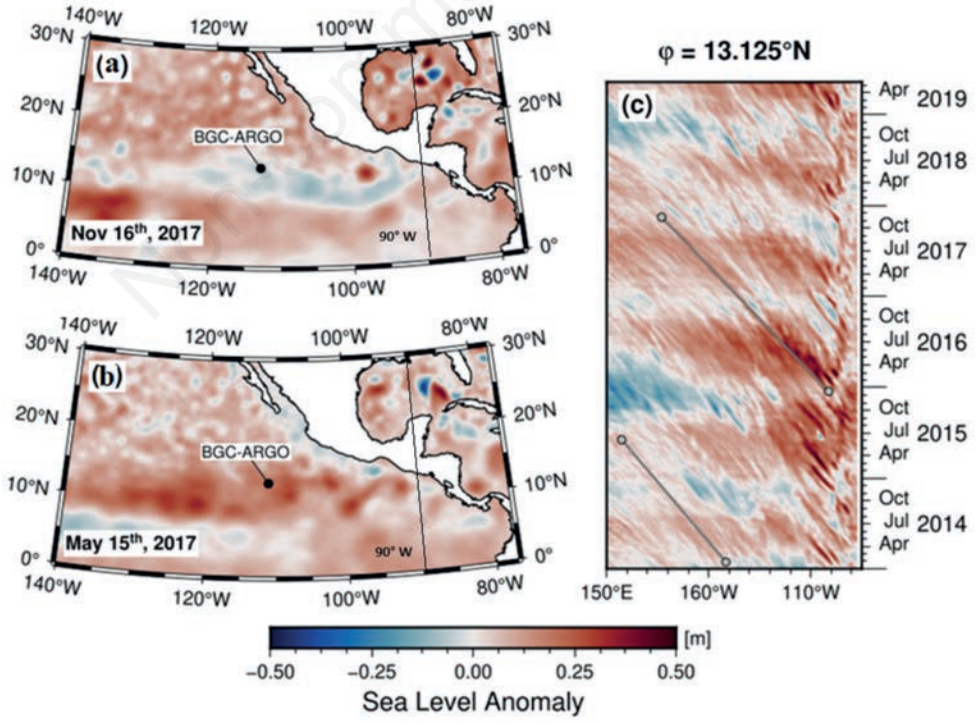

Figure 3. Spatial and temporal evolution of the Sea Level Anomaly (SLA) near the BGC-Argo float position. It is shown the spatial distribution of SLA on November 16th, 2017 (a) and May 15th, 2017 (b). A longitude-time plot at 13.125°N is shown in (c) with two examples of the lines used to estimate the phase speed of Rossby Waves.

to the temporal evolution of Z20, a comparison of the temporal variability of Ekman pumping and Z20 reveals a lag between the time series. Maximum Ekman pumping velocities occurred before those of Z20 (Figure 5b and 5c). with cross-correlation indicating when Z20 was lagged by 85 days (r=-0.3, p-value <0.05, n=239). This phase difference indicates that a local response of Z20 to wind cannot fully explain the observed temporal variability.

Throughout the analyzed record, Z20 observations displayed significant deviations from the annual signal and the predicted results derived from the LRWs model (Figure 5b). For instance, in October-November of 2017, Z20 anomalies reached -40 m instead of the -20 m predicted by the annual harmonic and the model (Figure 5b). It implies that the termocline was 20 m shallower than expected, likely due to processes with frequencies higher than the annual.

It is during these periods of significant departures from the annual cycle that chlorophyll-*a* substantially increased in the shallower chlorophyll-*a* maximum, resembling bursts or atypical events rather than a cyclic phenomenon (Figure 5). The annual cycle of the chlorophyll-*a* had an amplitude of 0.03 mg m^{-3}, accounting for the 4.6% of the total variance. The chlorophyll-*a* enhancements in November 2017 and December 2018 (Figure 4a and 5a) surpassed a concentration of 0.9 mg m^{-3} and lasted for 3 months. In standardized data terms, these short bursts of chlorophyll-*a* enhancements exceed the mean (0.34±0.1 mg m^{-3}) by more than 3 standard deviations.

LRWs model can explain the low-frequency variability of Z20, but not the higher-frequency variability. Here, we first present supporting information regarding the occurrence of LRWs with annual periods in the ETNP and analyze eddy occurrences in the studied region. It can be noted that there is a quite good correspondence between the spatial patterns of the annual cycle from

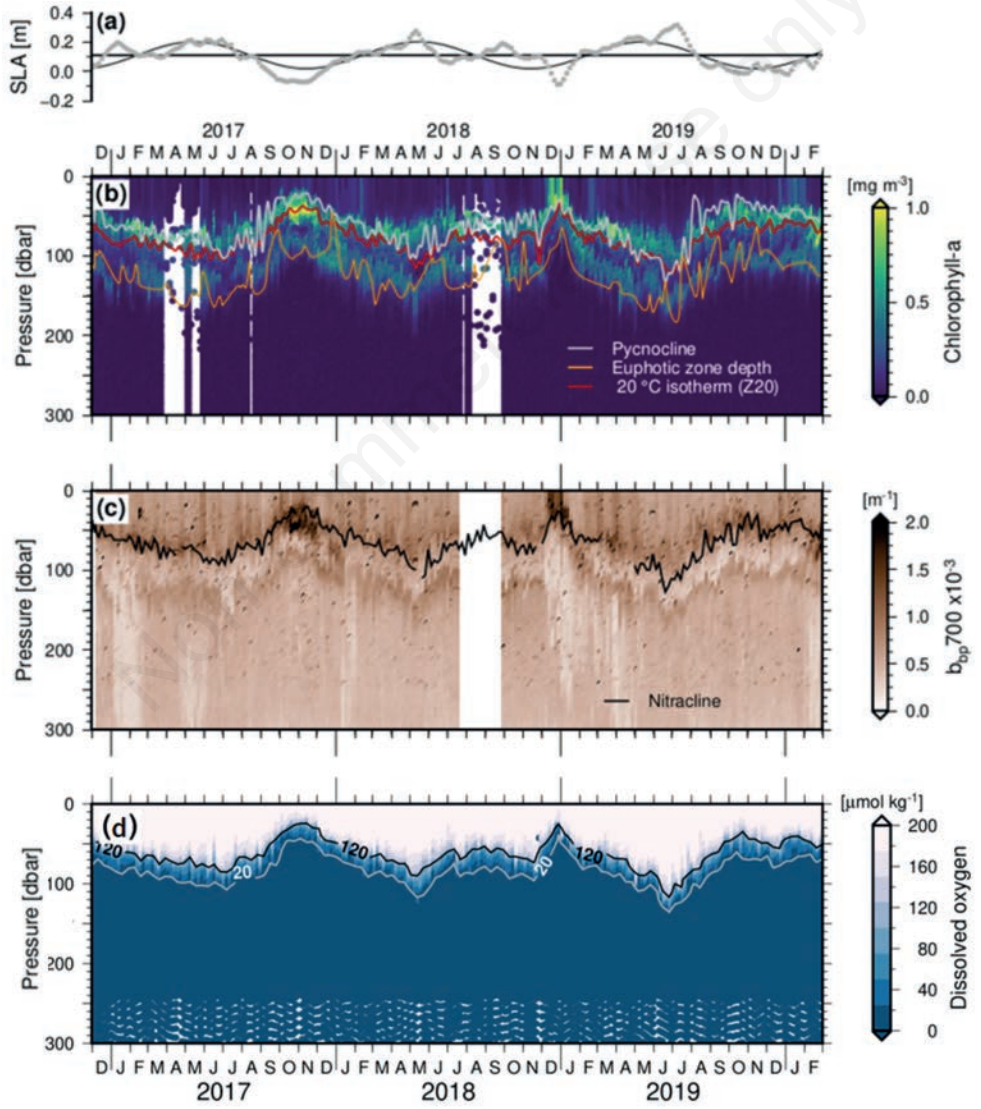

Figure 4. Temporal evolution of Sea Level Anomaly (SLA) represented by the gray line and the black line is the annual cycle of SLA (a), chlorophyll-*a*. (b), the particle backscattering coefficient measured at 124° and 700 nm wavelength (bbp700) in (c), and the dissolved oxygen (d). The position of the 20°C isotherm (Z20), pycnocline, nitracline and the euphotic zone depth are also shown.

sea level anomalies and the model presented in Figure 6. Thus, this provides supporting evidence to relate the low-frequency variability of the ETNP with the propagation of LRWs.

Secondly, the role of eddies in departures from the annual cycle is explored in Figure 7 where we classified the observations of SLA depending on whether the float was inside or outside eddies. For example, on January 15th, 2017 the float was inside an anticyclone, resulting in a positive SLA (Figure 7b), and hence a deeper thermocline. The opposite scenario was recorded on December 31st, 2018, during the influence of a cyclonic eddy (Figure 7c). However, some events with remarkable differences from the annual cycle were not associated with eddies, as can be noted on June 19th, 2019 (Figure 7d). During this event, the float was within a region of relatively strong positive anomalies extending from 112-124°W (~1200 km). As seen in Figure 7d, several eddies were detected inside this region of positive SLA, but the float was not within any of them or their edges (Figure 7a and d). Finally, this region with positive sea level anomalies, with a spatial extent of ~1200 km, originates at the coast and propagates westward.

Principal Component Analysis

We implemented a PCA to decompose the variability of conditions at the depth of each chlorophyll-*a* maximum (the oxic-CM and suboxic-CM), and most importantly to identify patterns of co-variability between variables. The variables used were the Dissolved Oxygen (DO), nitracline depth (Z_nitracline), daily integrated PAR (PAR), chlorophyll-*a* (chla), $b_{bp}700$ (b_{bp}), and the ratio between $b_{bp}700$: and chlorophyll-*a* (b_{bp}:chla). The results of the PCA are presented as bi-plots (Gabriel, 1971; Legendre and Legendre, 2012) in Figure 8, and

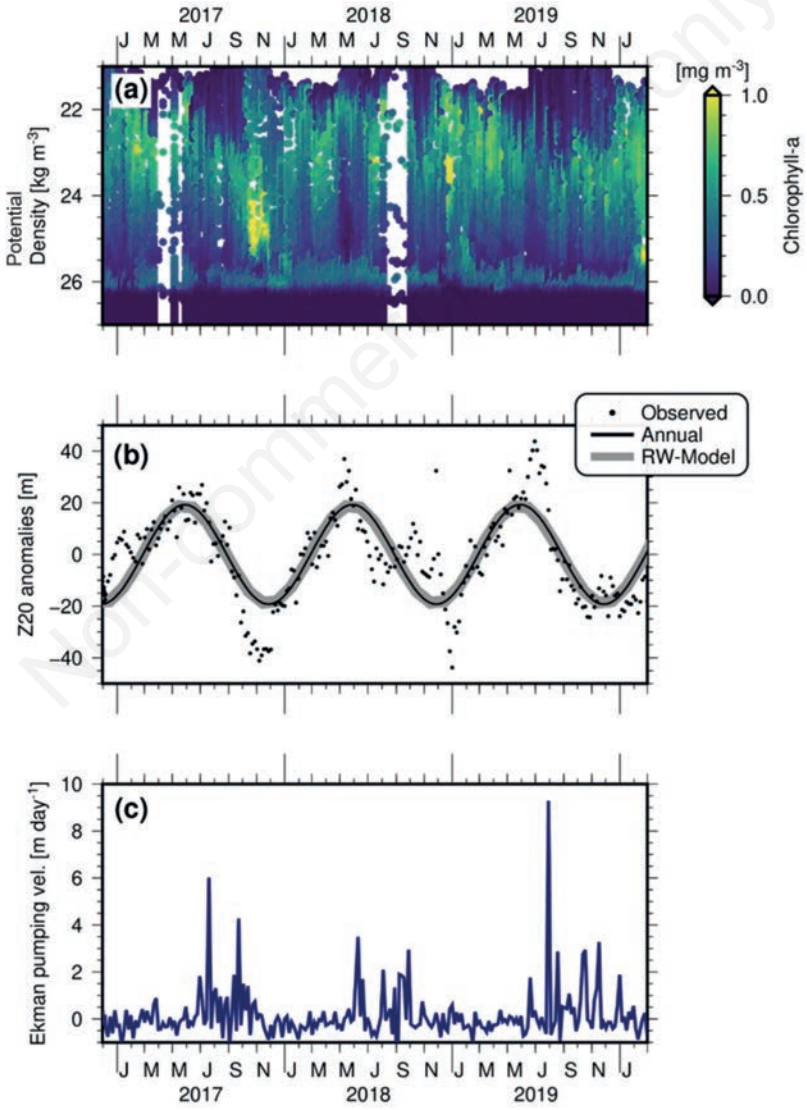

Figure 5. Temporal variability of chlorophyll-a (a), the depth of 20C isotherm: Z20 (b) and the Ekman pumping velocity (c). In (b) it is depicted the BGC-float observations of Z20 (dots), their annual harmonic (black line) and the estimated Z20 from a theoretical Rossby wave model (gray thick line).

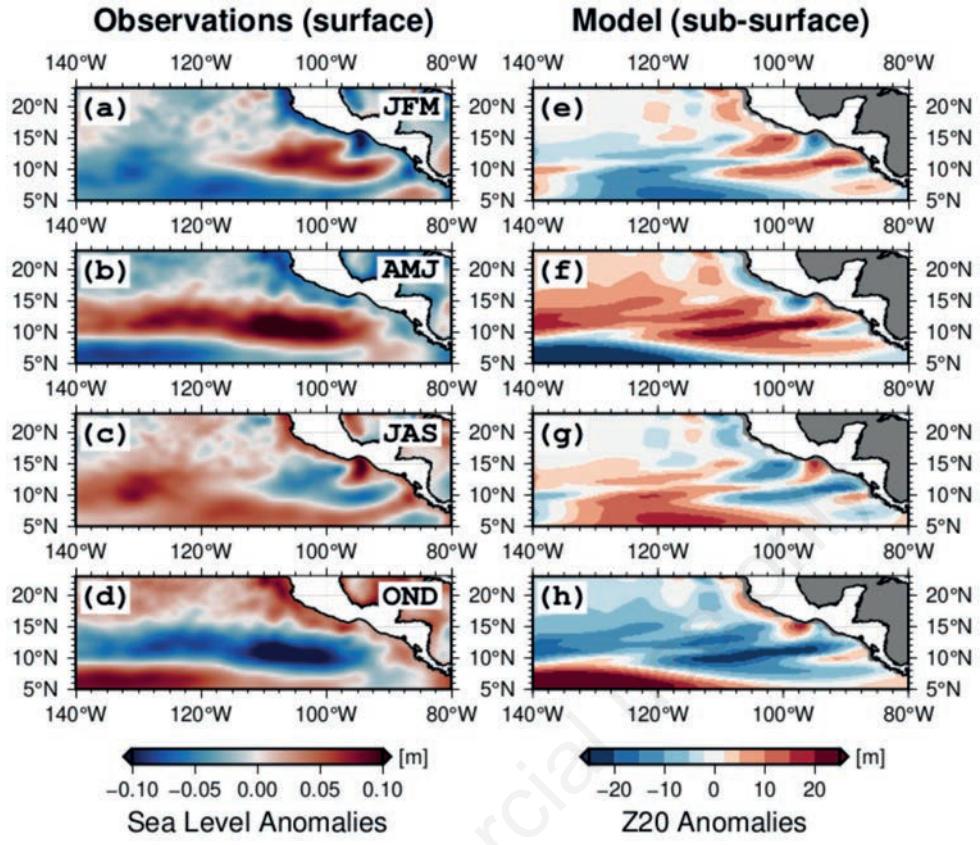

Figure 6. Comparison between the annual cycle from altimetry observations (a-d) and theoretically estimated from a Rossby wave model (e-h). The annual cycle of both datasets was quarterly averaged.

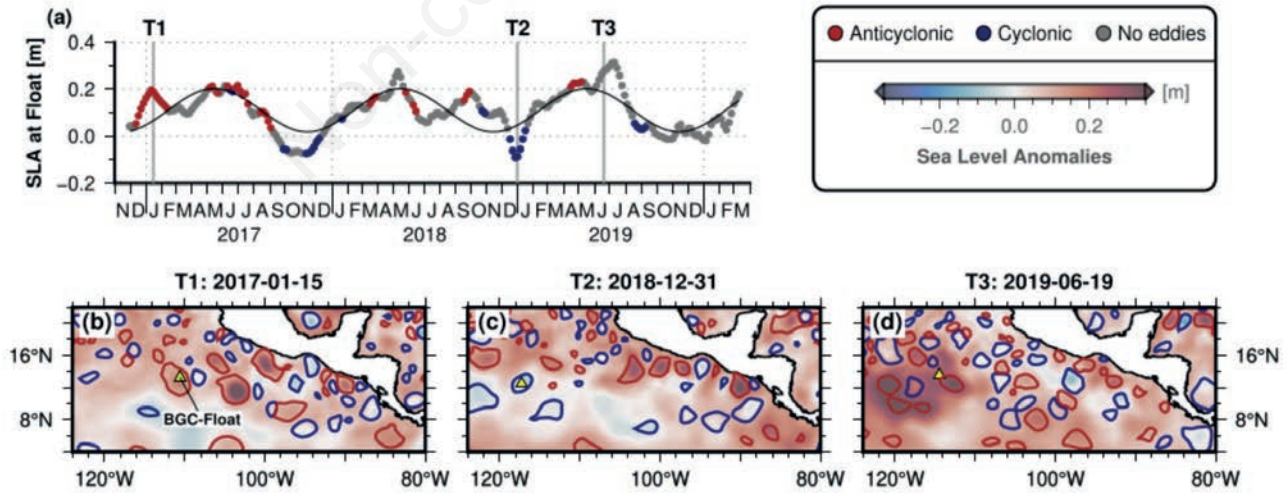

Figure 7. Temporal evolution of the Sea Level Anomaly (SLA) and occurrence of eddies on the float position. In (a) it is shown the SLA at the BGC-Argo float position. Each observation of SLA was classified and colored considering if the BGC-Argo float was outside of any Eddy (gray), inside anticyclonic (red points) or within cyclonic eddies (blue). The black line in (a) represents the annual cycle. Three temporal snapshots of the SLA (T1, T2, T3) are represented in the lower panels (b-d). The red and blue contours in the maps delineate spatial boundaries of anticyclonic and cyclonic eddies and the little white triangle is the position of the float. We do not screen eddies by lifespan or size.

the correlation coefficient of each variable and the statistical significance with a given principal component are shown in Tables 1 and 2.

In the bi-plots, the individual observations are projected into a nondimensional space defined by the Principal Components (PCs). In our case, the coordinates for the individual observations in each PC, are obtained by multiplying the eigenvectors (loadings) by the square root of the corresponding eigenvalues. The contribution of each variable (Z_nitracline, chlorophyll-*a*, $b_{bp}700$, *etc*.) is represented using arrows. In general terms, the angle between the arrows and the PCs is related to their correlation, ranging from 0° for a positive correlation and 180° for a negative association. An angle of 90° between an arrow and a given PC indicates no correlation. Variables with arrows in the same direction and with similar angles will have strong positive correlations. The arrow representation is employed to seek a physical/biological explanation for the mathematically constructed PCs.

The first PC of the oxic-CM accounts for 44.2% of the variance and is dominated by the contribution of $b_{bp}700$, chlorophyll-*a,* and the nitracline depth, which covaried (Figure 8a and Table 1). Along with this first PC, observations with the highest (intense red points at the left) and lowest (intense blue points at the right) Z20 values were separated, indicating that they are not seasonal events (Figure 8a). The second PC for the oxic-CM (22.2 % of the total variance), had the major contributions from the ratio $b_{bp}700$:chla, which were positively correlated with this axis (Figure 8a). Chlorophyll-*a* exhibited a negative correlation with the second PC (Table 1), suggesting that the second mode could be attributed to photoacclimation (chlorophyll-*a* increases when PAR decreases).

The pattern found after performing PCA with the conditions of the suboxic-CM was different (Figure 8b). In the first, PC Chlorophyll-*a*, $b_{bp}700$, and the ratio $b_{bp}700$:chla co-varied (36.6 % of the total variance) but, they were nearly orthogonal to the changes in PAR and nitracline depth, which were significantly associated with the second PC (Figure 8b and Table 2). Oxygen had a significant correlation with PC1 although it was low (Table 2).

The PCA conducted with the conditions of the oxic-CM suggests that the depth of the nitracline or the nutrient concentration is the main factor causing the chlorophyll-*a* and biomass enhancements, while light seems to have a limited effect. This behavior differs from those observed in oligotrophic regions, where irradiance drives seasonal changes in the chloro-

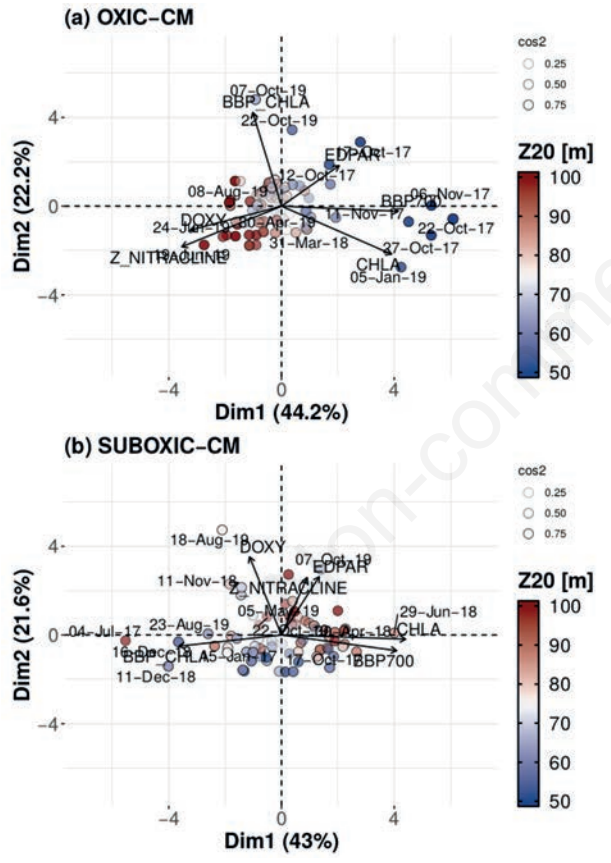

Figure 8. PCA bi-plots for the conditions associated with the oxic-CM (a) and the suboxic-CM (b). Each dot represents an individual observation projected into PCs, which are linear combinations of the original variables: chlorophyll-*a* (chl), particle backscattering coefficient (bbp: proxy of carbon), nitracline depth (z_nit), daily integrated PAR (PAR), dissolved oxygen (DO), and the ratio between bpp700 and chlorophyll-*a* (bbp:chl). Each dot is colored according to the vertical position of the 20°C isotherm (Z20).

Table 1. Pearson's correlation coefficients between the Principal Components (PCs) and the original variables describing the conditions at the oxic-CM. Correlations marked with the star symbol (*) were statistically significant at the 95% confidence level.

Variable	Oxic-CM, PC-1	Oxic_CM, PC-2
b_{bp}	0.87*	-0.05
chl	0.82*	-0.45*
b_{bp}:chl	-0.21	0.88*
Z_nit	-0.74*	-0.38*
PAR	0.43*	0.38*
DO	-0.68*	-0.23*

CM, chlorophyll-*a* maximum; PAR, photosynthetically activeradiation; DO, dissolved oxygen.

Table 2. Pearson's correlation coefficients between the Principal Components (PCs) and the original variables describing the conditions at the suboxic-CM. Correlations marked with the star symbol (*) were statistically significant at the 95% confidence level.

Variable	Suboxic-CM, PC1	Suboxic-CM, PC2
b_{bp}	0.90*	-0.165
chl	0.97*	-0.04
b_{bp}:chl	-0.80*	-0.110
Z_nit	0.20	0.57*
PAR	0.30*	0.58*
DO	-0.25*	0.78*

CM, chlorophyll-*a* maximum; PAR, photosynthetically active radiation; DO, dissolved oxygen.

phyll-*a* maximum, which follows the movements of isolumes. For this reason, we plotted the chlorophyll-*a* as a function of PAR (Figure 9). We first compared the mean chlorophyll-*a* profiles gathered during April-June and from October-December. This represents two contrasting conditions in which the chlorophyll-*a* maxima reach their deepest and shallowest positions along the seasonal cycle. The chlorophyll-*a* during these contrasting conditions was quite similar, although the PAR changed remarkably with the maximum during April-June and the minimum in October-December (Figure 9a). In the case of the enhancement events, the PAR does not exceed the 1 molQ m^{-2} d^{-1} at the center of the oxic-CM, but it seems to cover a wider range of PAR values than in normal conditions (Figure 9b).

Discussion

The analysis presented here is supported by three years of measurements obtained by a BGC-ARGO. This kind of instrumentation is providing an unprecedented view of relevant biogeochemical processes, including those regulating chlorophyll-*a* and phytoplankton growth in the world oceans (*e.g.* Mignot *et al.*, 2014; Barbieux *et al.*, 2018). Using BGC-ARGO floats in the Arabian Sea OMZ, researchers have identified two chlorophyll maxima regulated by propagating LWRs (Ravichandran *et al.*, 2012). However, in the ETNP, this is the first time there is a sufficiently long time series to resolve those processes and, simultaneously, a data set that allows studying the role of light and nutrients in the dynamic of the phytoplankton communities. Here we will discuss the effects of physical phenomena on the vertical distribution of properties, and then we will address the implications for the variability of chlorophyll-*a*.

Several physical phenomena can be considered to explain the thermocline movements in an annual cycle. For example, mesoscale eddies (hundreds of km in diameter), the local Ekman pumping alone, and the propagation of LRWs (~900 km). Mesoscale eddies can be easily discarded to explain the low-frequency variability because they are not expected to cause an annual signal, as demonstrated in Figure 7. On the other hand, if the thermocline responds directly to local wind forcing, we would expect a high correlation with zero or short lag. However, that was not the case and the thermocline lagged by 2.8 months from the Ekman pumping velocity, supporting the idea that the thermocline responds to a remote forcing, as previously suggested by Fiedler and Talley (2006). The remote forcing can be the pattern of LRWs, whose occurrence in the ETNP is supported by the large-scale pattern in SLA (Figure 3a and b), the westward propagating signals at phase speeds characterizing LRWs (Figure 3c), and also given the correspondence between the theoretical LRWs model and observations of Z20 and SLA (Figure 5 and 6). The occurrence of annual Rossby waves and their effect on the low-frequency variability of the thermocline is not new, and has been extensively documented in previous works (Meyers, 1979; Kessler, 1990;

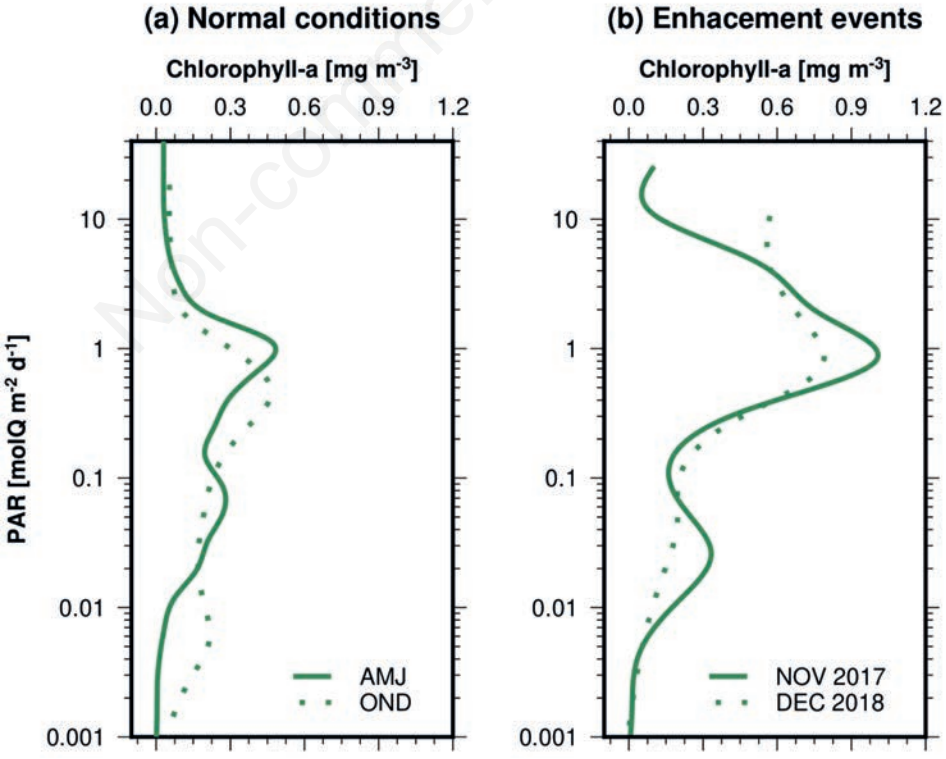

Figure 9. Distribution of chlorophyll-a as a function of daily integrated PAR. Chlorophyll-*a* profiles gathered on "normal" conditions between April-June (AMJ) and October-December (OND) are compared to represent differences along the seasonal cycle (a). The enhancement events observed during November 2017 and December of 2018 are represented in (b).

Chelton and Schlax, 1996; Qiu *et al*., 1997; Capotondi *et al*., 2003; Polito and Liu, 2003). Hence, at 13°N the thermocline/nitracline annual cycle is driven by the propagation of LRW forced by the wind stress curl as a cumulative forcing from the eastern coast to the open ocean, rather than a direct effect of the wind by Ekman pumping alone.

The annual cycle of the thermocline/nitracline accounts for a considerable portion of the total variance, but other events at lower periods (~4 months) were observed and they caused remarkable differences from the annual cycle (Figure 5b). Again, we can attribute these events to several processes. We first assessed the mesoscale eddies because the BGC-Argo float was near the path of eddies generated in Tehuantepec by the Central America wind jets (Chelton *et al*., 2007; Aleynik *et al*., 2017). Our analysis showed that several eddies pass over the BGC-Argo float (Figure 7), and some of them seem to cause strong departures from the annual cycle. Nonetheless, other events were not associated with eddies, such as the event occurring on June 19th, 2019. In this case, strong departures from the annual cycle corresponded to a larger scale process than eddies (Figure 7d), originating at the coast and propagating westward. Given these characteristics, the phenomenon could be associated with Rossby waves of shorter periods than annual, which have been reported to occur in the ETNP (Polito and Liu, 2003). It seems that eddies propagate along with these Rossby waves, as has been demonstrated previously (Polito and Sato, 2015). In summary, the propagation of LRWs of the annual period generates a "background" signal over the thermocline/nitracline that is modulated by higher frequency processes, including, but not limited to mesoscale eddies.

We have shown that the thermocline/nitracline and isopycnals are affected by the occurrence of several processes. Here, we are going to focus on the implications it has on the chlorophyll-*a* field. Firstly, in the analyzed dataset from the BGC-float, the vertical distribution of chlorophyll-*a* presented two persistent maxima, which coincided with a local increase in the bbp700 signal: a proxy of the particulate organic carbon or phytoplankton biomass (Stramski *et al.*, 2008; Boss *et al*., 2015). Consequently, the chlorophyll-*a* maxima can be interpreted as phytoplankton biomass maxima with a remarkable depth variability (Figure 4). The vertical displacements of the maxima were synchronized, following the evolution of SLA, and the temporal variability of the thermocline/nitracline (Figure 4).

Because both Rossby waves and eddies modify the position of isopycnals in the water column, they can also alter the vertical distributions of nutrients, and consequently the chlorophyll-*a*. However, the movement of isopycnals can affect the chlorophyll-*a* through either mechanical action if phytoplankton is associated with a specific isopycnal's surface, or as a biological response of phytoplankton to changes in nutrients and light. Thus, if chlorophyll-*a* is plotted in density space (Figure 5a), where the effects of circulation are removed, the chlorophyll-*a* maxima will appear flat over time if only mechanical action occurs in response to the isopycnals movements. It is noticeable that the shallower chlorophyll-*a* maximum, which we call the oxic-CM, oscillated in the density space. In contrast, the deeper maximum or the suboxic-CM remains tightly coupled to the 26 kg m^{-3} isopycnal. The oxic-CM intensifies when it moves to denser waters, possibly in response to an increase in the nutrient supply (Figure 5a). By contrast, the suboxic-CM is only mechanically displaced (Figure 5a). Hence, each maximum has a different response to the isopycnals movements.

A more detailed view of the factors controlling the evolution of each chlorophyll-*a* maximum is based on the interpretation of the PCA (Figure 8). In the case of the oxic-CM, the first PC was dominated by the co-variability between chlorophyll-*a*, bbp700, and the variability in nitracline depth, supporting the idea that changes in chlorophyll-*a* are controlled by the nitrate supply (Figures 4 and 8). Given these observations and considering that the oxic-CM is located near the nitracline, we suggest that it fits into the typical stable water structure proposed by Cullen (2015) from meso and eutrophic conditions, in which the movements of the nitracline control the chlorophyll-*a* concentration, the biomass, and the primary production.

The explanation above implies that the variability of chlorophyll-*a* in the oxic-CM is driven by nutrients rather than by light. Light-driven cycles are common in oligotrophic environments. For instance, in the North Pacific subtropical gyre, the chlorophyll-*a* maximum follows the depth of the isolumes, exhibiting a seasonal cycle in the chlorophyll-*a* concentration: it intensifies during the summer when light penetrates deeper into the water column, while during the winter, chlorophyll-*a* decreases due to light limitation, even when nutrients are available (Letelier *et al*., 2004). In contrast, in our study region, the seasonal cycle of the chlorophyll-*a* at the oxic-CM had a very low amplitude, accounting for less than 5% of the total variance, and the chlorophyll-*a* maxima do not align with a specific isolume (Figure 9).

Chlorophyll-*a* enhancements occurred at higher PAR values than the expected mean, but did not exceed the maximum mean value observed during April-June (~1 molQ m^{-2} day^{-1}). During enhancements events, chlorophyll-*a* increased by a factor of 4, which is difficult to explain solely considering the observed PAR variability. Thus, the dynamics of the oxic-CM differ from those of oligotrophic conditions, which are seasonally light-driven. Instead, it aligns with a typically stable water structure scenario, where chlorophyll-*a* is primarily controlled by nutrient supply (Cullen 2015).

Here, we will discuss the second PC of the oxic-CM, which was dominated by changes in the b_{bp}:chla ratio, and presented a weak negative correlation between chlorophyll-*a* and PAR. This could be attributed to photoacclimation, but the profiles of chlorophyll-*a* as a function of PAR indicates that the chlorophyll-*a* concentration remains unchanged despite variability in light under seasonally contrasting conditions (Figure 9a). Hence, we do not find strong evidence of photoacclimation, and the second PC could be associated with changes in phytoplankton community composition. Assessing this is challenging with the current datasets but could be explored in future works on phytoplankton of the ETNP.

According to our analysis (Figure 8 and Table 1), dissolved oxygen is another variable that appears to be related to the chlorophyll-*a* enhancements of the oxic-CM. Generally, the oxic-CM significantly intensifies when denser and deeper waters move toward the surface. Given the strong oxygen gradients of the OMZ, this implies a substantial decrease in the dissolved oxygen, ranging from a maximum of 187.3 µmol O_2 kg^{-1} during "normal conditions" to a minimum of 20.6 µmol O_2 kg^{-1} during enhancements. The significant decrease in oxygen could limit the distribution and abundance of organisms at the depth of the oxic-CM, thereby reducing grazing pressure: a source of phyto-

plankton cell loss. While these changes in phytoplankton loss have been considered relevant factors affecting phytoplankton accumulation (Behrenfeld and Boss 2014, Arteaga *et al*., 2020). they may not be the primary cause here, but they could contribute to some degree.

The suboxic-CM can be considered a special case, exhibiting a pattern that deviates from the typical stable water structure. It was located below the nitracline at a depth of 118 meters, where oxygen concentrations were below 5 µmol kg^{-1}, and the mean PAR was 0.26 molQ m^{-2} d^{-1} (equivalent to 0.6% of irradiance just below the sea surface): conditions favoring the growth of low light-adapted ecotypes of *Prochlorococcus* in the OMZs (Goericke *et al*., 2000; Lavin *et al*., 2010; Garcia-Robledo *et al*., 2017).

In the multivariate analysis of the suboxic-CM conditions, the chlorophyll-*a*, bbp700, and the ratio bbp700: chla were the dominant variables in the first component, nearly orthogonal (~90° angle) to the second principal component, where PAR and nitracline depth dominate the variability (Figure 8b). Thus, chlorophyll-*a* and bbp700 do not co-vary with nitrate and light. Oxygen showed a low correlation with the second component, and there was a clear pattern explaining the variability of chlorophyll-*a* or bbp700 in the suboxic-CM. We considered that other variables, such as biological interactions between *Prochlorococcus* and other bacteria of the OMZ, could be responsible for the maintenance of the suboxic-CM, but further assessment is needed.

Finally, we highlight the persistence of the suboxic-CM observed in the BGC-float data set, present in 96.9% of all profiles (Figure 2). This persistence was also reported in the Pacific off Mexico between 16-21°N (Márquez-Artavia *et al*., 2019), and here it is corroborated for a more extended region of the ETNP. In contrast, the suboxic-CM seems to occur sporadically in the Arabian Sea, and the eastern tropical South Pacific (Whitmire *et al*., 2009; Ravichandran *et al*., 2012; Wojtasiewicz *et al*., 2018). The reasons for the persistence of the suboxic-CM persists in the ETNP are not well understood, but it demonstrates differences in the dynamics of the OMZs across the global ocean.

Future studies on the process affecting the phytoplankton communities of the OMZ are required. There is a definite need for more instruments to measure regularly in the OMZs. For example, direct measurements of nitrate concentration are needed to shed more light on the use of this nutrient by the phytoplankton populations, especially in the suboxic waters of the OMZ.

Conclusions

The findings of this study are consistent with previous research highlighting the significant contribution of annual LRWs to the variability of thermocline/nitracline depth, which in turn affects the movement of isopycnals. However, we also identified other physical processes with higher frequencies than annual variations (*e.g.* mesoscale eddies and shorter-period Rossby waves), which modulate the background annual signal. Constructive interactions among these processes can lead to extraordinary events, characterized by a shallow nitracline, and increased nutrient supply into the euphotic zone. These extraordinary events are expected to happen more frequently during October-December when annual LRWs displace the nitracline closer to the surface along with the annual cycle.

The response of each chlorophyll-*a* maximum to the vertical displacements of the isopycnals varied. The oxic-CM appears to be primarily influenced by increased nutrient concentration and possibly reduced grazing pressure due to significant changes in dissolved oxygen. This was observed during short periods of intensified chlorophyll-*a* and biomass (b_{bp}) suggesting enhanced phytoplankton growth. A secondary variation in the oxic-CM, dominated by changes in the b_{bp}:chla ratio may be linked to changes in phytoplankton community composition, as there was evidence of photoacclimation in response to seasonal changes in irradiance. Lastly, the deeper chlorophyll-*a* maximum, referred (suboxic-CM), persisted at a depth where PAR can sustain net growth of low-light adapted *Prochlorococcus* ecotypes. This deeper chlorophyll-*a* maximum was displaced mechanically along with the isopycnals and its temporal evolution appears to be decoupled from irradiance and nitrate levels.

Appendix: the linear Long Rossby Wave model

The linear model simulating the thermocline depth variability by the effect of LRW, has a solution with two terms: i) the wind component (h_W) associated to the wind stress curl forcing (τ) and, ii) LRWs radiating from the eastern boundary (h_B) due to the variability of the thermocline depth near to the coast (h_E). Solution ii is important only near the coast and quickly decayed in the open ocean.

$$h_W(x,t) = \frac{-1}{c_r}\int_{x_E}^{x} e^{\frac{-R}{c_r}(x-x')} \nabla \times \left[\tau\frac{\left(x',t-\frac{x-x'}{c_r}\right)}{f\rho}\right] dx' \quad \text{(i)}$$

$$h_B(x,t) = e^{\frac{-R}{c_r}(x-x_E)} h_E\left(t-\frac{x-x_E}{c_r}\right) \quad \text{(ii)}$$

where c_r denotes phase speed of LRWs ($-\beta c^2/f^2$), R is the damping timescale, f is the Coriolis parameter and ρ is considered as a mean ocean density (1027 kg m^{-3}). The value for the gravitational waves speed was $c = 2\,\frac{m}{s}$. The lower limit of the integration, x_E, is the longitude at the eastern boundary and the values of all parameters are the same used previously by Kessler (2016) for consistency. The boundary condition (h_B) was the annual cycle of the thermocline, averaged in the first four degrees from the coast.

We used wind data from the Cross-Calibrated Multiplatform version 2 (CCMPv2), between the period 2010-2018. From this data, the annual cycle of the wind stress curl has been estimated. The wind dataset has a spatial resolution of 0.25°x0.25° and it was acquired from Remote Sensing Systems (www.remss.com). We used the EN4 gridded dataset (Good *et al*., 2013) to compute the boundary condition (h_B). EN4 dataset is available at the Met office-UK website (https://www.metoffice.gov.uk/hadobs/en4/).

References

Aleynik D, Inall ME, Dale A, Vink A, 2017. Impact of remotely generated eddies on plume dispersion at abyssal mining sites in the Pacific. Sci. Rep. 7:1-14.

Antoine D, André J-M, Morel A, 1996. Oceanic primary production 2. Estimation at global scale from satellite (coastal zone color scanner) chlorophyll. Global Biogeochem. Cycles 10:57-69.

Arteaga LA, Boss E, Behrenfeld MJ et al., 2020. Seasonal modulation of phytoplankton biomass in the Southern Ocean. Nat Commun. 11:5364.

Barbieux M, Uitz J, Bricaud A et al., 2018. Assessing the variability in the relationship between the particulate backscattering coefficient and the chlorophyll-a concentration from a global biogeochemical-Argo database. J. Geophys. Res. Ocean. 123:1229-50.

Barron CN, Kara AB, Jacobs GA, 2009. Objective estimates of westward Rossby wave and eddy propagation from sea surface height analyses. J. Geophys. Res. Ocean. 114:1-18.

Behrenfeld MJ, Boss ES, 2014. Resurrecting the ecological underpinnings of ocean plankton blooms. Ann. Rev. Mar. Sci. 6:167-94.

Belonenko TV, Bashmachnikov IL, Kubryakov AA, 2018. Horizontal advection of temperature and salinity by Rossby waves in the North Pacific. Int. J. Remote Sens. 39:2177-88.

Bernades H, Suryoputro AAD, Wirasatriya A et al., 2021. The effect of Ekman mass transport and Ekman pumping velocity on the variability of sea surface temperature in the Arafura Sea. IOP Conference Series: Earth and Environmental Science. 919:012026.

Bittig H, Wong A, Plant J, CORIOLIS-ADMT, 2018. BGC-Argo synthetic profile file processing and format on Coriolis GDAC. Available from: https://archimer.ifremer.fr/doc/00445/55637/

Boss E, Häentjens N, 2016. Primer regarding measurements of chlorophyll fluorescence and the backscattering coefficient with WETLabs FLBB on profiling floats. Available from: https://soccom.princeton.edu/sites/g/files/toruqf5341/files/documents/SOCCOM_2016-1_Bio-optics-primer.pdf

Boss E, Pegau WS, 2001. Relationship of light scattering at an angle in the backward direction to the backscattering coefficient. Appl. Opt. 40:5503.

Boss E, Stramski D, Bergmann T et al., 2015. Why should we measure the optical backscattering coefficient? Oceanography 17:44-9.

Briggs N, Perry MJ, Cetinić I et al., 2011. High-resolution observations of aggregate flux during a sub-polar North Atlantic spring bloom. Deep. Res. Part I Oceanogr. Res. Pap. 58:1031-9.

Capotondi A, Alexander MA, Deser C, 2003. Why are there Rossby wave maxima in the Pacific at 10 degrees S and 13 degrees N? J. Phys. Oceanogr. 33:1549-63.

Chelton DB, Schlax MG, 1996. Global observations of oceanic Rossby waves. Science. 272:234-8.

Chelton DB, Schlax MG, Samelson RM, de Szoeke RA, 2007. Global observations of large oceanic eddies. Geophys. Res. Lett. 34:1-5.

Cullen JJ, 2015. Subsurface chlorophyll maximum layers: enduring enigma or mystery solved? Ann. Rev. Mar. Sci. 7: 207-39.

Fiedler PC, Talley LD, 2006. Hydrography of the eastern tropical Pacific: a review. Prog. Oceanogr. 69:143-80.

Gabriel KR, 1971. The biplot graphic display of matrices with application to principal component analysis. Biometrika 58:453-67.

Garcia-Robledo E, Padilla CC, Aldunate M et al., 2017. Cryptic oxygen cycling in anoxic marine zones. Proc. Natl. Acad. Sci. 114:8319-24.

Glatt I, Dörnbrac, A, Jones S et al., 2011. Utility of Hovmöller diagrams to diagnose Rossby wave trains. Tellus A. 63:991-1006.

Godínez VM, Beier E, Lavín MF, Kurczyn JA, 2010. Circulation at the entrance of the Gulf of California from satellite altimeter and hydrographic observations. J. Geophys. Res. Ocean. 115:1-15.

Goericke R, Olson RJ, Shalapyonok A., 2000. A novel niche for Prochlorococcus sp. in the low-light suboxic environments in the Arabian Sea and the Eastern Tropical North Pacific. Deep. Res. I 47:1183-205.

Good SA, Martin MJ, Rayner NA, 2013. EN4: Quality controlled ocean temperature and salinity profiles and monthly objective analyses with uncertainty estimates. J. Geophys. Res. Ocean. 118:6704-16.

Kessler WS, 1990. Observations of Long Rossby Waves in the Northern Tropical Pacific. J. Geophys. Res. 95:5183-217.

Kessler WS, 2006. The circulation of the Eastern Tropical Pacific: a review. Prog. Oceanogr. 69:181-217.

Killworth PD, Cipollini P, Uz BM, Blundell JR, 2004. Physical and biological mechanisms for planetary waves observed in satellite-derived chlorophyll. J. Geophys. Res. C Ocean. 109:1-18.

Kurian J, Colas F, Capet X et al., 2011. Eddy properties in the California Current System. J. Geophys. Res. 116:C08027.

Lalli C, Parsons TR, 1997. Biological oceanography: an introduction. Elsevier, Amsterdam, The Netherlands. 314 pp.

Lavin P, González B, Santibáñez JF et al., 2010. Novel lineages of Prochlorococcus thrive within the oxygen minimum zone of the eastern tropical South Pacific. Environ. Microbiol. Rep. 2:728-38.

Legendre P, Legendre L, 2012. Numerical ecology. Elsevier, Amsterdam, The Netherlands. 1006 pp.

Letelier RM, Karl DM, Abbott MR, Bidigare RR, 2004. Light driven seasonal patterns of chlorophyll and nitrate in the lower euphotic zone of the North Pacific Subtropical Gyre. Limnol. Oceanogr. 49:508-19.

Li X, Yang D, Yang J et al., 2021. Validation of NOAA CYGNSS wind speed product with the CCMP data. Remote Sensing. 13:1832.

Márquez-Artavia A, Sánchez-Velasco L, Barton ED et al., 2019. A suboxic chlorophyll-a maximum persists within the Pacific oxygen minimum zone off Mexico. Deep. Res. Part II Top. Stud. Oceanogr. 169-170:104686.

Martinez-Vicente V, Dall'Olmo G, Tarran G et al., 2013. Optical backscattering is correlated with phytoplankton carbon across the Atlantic Ocean. Geophys. Res. Lett. 40:1154-8.

Mason E, Pascual A, McWilliams JC, 2014. A new sea surface height-based code for oceanic mesoscale eddy tracking. J. Atmos. Ocean. Technol. 31:1181-8.

Mcdougall TJ, Barker PM, 2017. Getting started with TEOS-10 and the Gibbs Seawater (GSW) Oceanographic Toolbox. Available from: https://www.teos-10.org/pubs/Getting_Started.pdf

McGillicuddy DJ, 2016. Mechanisms of physical-biological-biogeochemical interaction at the oceanic mesoscale. Annual Review of Marine Science. 8:125-59.

McGillicuddy DJ, Anderson L, Bates NR et al., 2007. Eddy/wind interactions stimulate extraordinary mid-ocean plankton blooms. Science. 316:1021-6.

Meyers G, 1979. On the annual Rossby wave in the Tropical North Pacific Ocean. J. Phys. Oceanogr. 9:663-74.

Mignot A, Claustre H, D'Ortenzio F et al., 2011. From the shape

of the vertical profile of in vivo fluorescence to Chlorophyll-a concentration. Biogeosciences 8:2391-406.

Mignot A, Claustre H, Uitz J et al., 2014. Understanding the seasonal dynamics and the deep chlorophyll maximum in oligotrophic environments: a Bio-Argo investigation. AGU. Glob. Biogeochem. Cycles. 28:856-76.

Mignot A, Ferrari R, Claustre H, 2018. Floats with bio-optical sensors reveal what processes trigger the North Atlantic bloom. Nat. Commun. 9:1-9.

Moore LR, Goericke R, Chisholm SW, 1995. Comparative physiology of Synechococcus and Prochlorococcus: Influence of light and temperature on growth, pigments, fluorescence and absorptive properties. Mar. Ecol. Prog. Ser. 116:259-75.

Muñoz-Anderson M, Millán-Núñez R, Hernández-Walls R et al., 2015. Fitting vertical chlorophyll profiles in the California Current using two Gaussian curves. Limnol. Oceanogr. Methods 13:416-24.

Ollitrault M, Rannou J-P, 2013. ANDRO : an Argo-based deep displacement dataset. J. Atmos 30: 759-88.

Organelli E, Claustre H, Bricaud A et al., 2016. A novel near-real-time quality-control procedure for radiometric profiles measured by bio-Argo floats: Protocols and performances. J. Atmos. Ocean. Technol. 33:937-51.

Pennington JT, Mahoney KL, Kuwahara VS et al., 2006. Primary production in the eastern tropical Pacific: a review. Prog. Oceanogr. 69:285-317.

Polito PS, Liu WT, 2003. Global characterization of Rossby waves at several spectral bands. J. Geophys. Res. 108: 3018.

Polito PS, Sato OT, 2015. Do eddies ride on Rossby waves? J. Geophys. Res. Oceans. 120:5417-35.

Poteau A, Organelli E, National I, Xing X, 2019. Quality control for Biogeochemical-Argo radiometry. Available from: https://archimer.ifremer.fr/doc/00513/62466/66773.pdf

Qiu B, Miao W, Müller P, 1997. Propagation and decay of forced and free baroclinic Rossby waves in off-equatorial oceans. J. Phys. Oceanogr. 27:2405-17.

Rasse R, Dall'Olmo G, Graff J et al., 2017. Evaluating optical proxies of particulate organic carbon across the surface Atlantic ocean. Front. Mar. Sci. 4:1-18.

Ravichandran M, Girishkumar MS, Riser S, 2012. Observed variability of chlorophyll-a using Argo profiling floats in the southeastern Arabian Sea. Deep. Res. Part I Oceanogr. Res. Pap. 65:15-25.

Rabinovich E, Govindjee, 1969. Photosynthesis. Available from: https://www.life.illinois.edu/govindjee/Electronic%20Publications/Books/Photosynthesis.pdf

R Core Team, 2018. R: a language and environment for statistical computing. R Foundation for Statistical Computing, Vienna, Austria. Available from: https://www.R-project.org/

Rembauville M, Briggs N, Ardyna M et al., 2017. Plankton assemblage estimated with BGC-Argo floats in the Southern Ocean: implications for seasonal successions and particle export. J. Geophys. Res. Ocean. 122:8278-92.

Ripa P, 2002. Least squares data fitting. Ciencias Mar. 28:79-105.

Roesler C, Uitz J, Claustre H et al., 2017. Recommendations for obtaining unbiased chlorophyll estimates from in situ chlorophyll fluorometers: A global analysis of WET Labs ECO sensors. Limnol. Oceanogr. Methods 15:572-85.

Sakamoto CM, Karl DM, Jannasch, HW et al., 2004. Influence of Rossby waves on nutrient dynamics and the plankton community structure in the North Pacific subtropical gyre. J. Geophys. Res. C Ocean. 109.

Sathyendranath S, Brewin RJW, Brockmann C et al*.,* 2019. An ocean-colour time series for use in climate studies: the experience of the Ocean-Colour Climate Change Initiative (OC-CCI). Sensors. 19:4285.

Sauzède R, Bittig HC, Claustre H et al., 2017. Estimates of water-column nutrient concentrations and carbonate system parameters in the global ocean : a novel approach based on neural networks. Front. Mar. Sci. 4:1-17.

Schmechtig C, Boss ES, Briggs NT et al., 2019. BGC Argo quality control manual for particles backscattering. Available from: https://archimer.ifremer.fr/doc/00491/60262/63668.pdf

Schmechtig C, Claustre H, Poteau A et al, 2023. Bio-Argo quality control manual for Chlorophyll-a concentration. Available from: https://archimer.ifremer.fr/doc/00243/35385/60181.pdf

Schmechtig C, Poteau A, Claustre H et al., 2018. Processing BGC-Argo particle backscattering at the DAC level. Available from: https://archimer.ifremer.fr/doc/00283/39459/56146.pdf

Sébastien L, Josse J, Husson F, 2008. FactoMineR: An R Packages for Multivariate Analysis. J. Stat. Softw. 25:1-18.

Siegel DA, McGillicuddy DJ Jr., Fields EA, 1999. Mesoscale eddies, satellite altimetry, and new production in the Sargasso Sea. J. Geophys. Res. 104:13359-79.

Stramski D, Boss E, Bogucki D, Voss KJ, 2004. The role of seawater constituents in light backscattering in the ocean. Prog. Oceanogr. 61:27-56.

Stramski D, Reynolds RA, Babin M et al., 2008. Relationships between the surface concentration of particulate organic carbon and optical properties in the eastern South Pacific and eastern Atlantic Oceans. Biogeosciences 5:171-201.

Uz BM, Yoder JA, Osychny V, 2001. Pumping of nutrients to ocean surface waters by the action of propagating planetary waves. Nature 409:597-600.

Watanabe WB, Polito PS, da Silveira ICA, 2016. Can a minimalist model of wind forced baroclinic Rossby waves produce reasonable results? Ocean Dyn. 66:539-48.

Whitmire AL, Letelier RM, Villagrán V, Ulloa O, 2009. Autonomous observations of in vivo fluorescence and particle backscattering in an oceanic oxygen minimum zone. Opt. Express 17:21992-2004.

Wojtasiewicz B, Trull TW, Udaya Bhaskar TVS et al., 2018. Autonomous profiling float observations reveal the dynamics of deep biomass distributions in the denitrifying oxygen minimum zone of the Arabian Sea. J. Mar. Syst. 207:103103.